Cement and Concrete Composites 124 (2021) 104262

Contents lists available at ScienceDirect

Cement and Concrete Composites

journal homepage: www.elsevier.com/locate/cemconcomp

Research Paper

On the optimization of BOF slag hydration kinetics

A.M. Kaja [a], S. Melzer [b], H.J.H. Brouwers [a], Qingliang Yu [a,c,*]

[a] Department of the Built Environment, Eindhoven University of Technology, Eindhoven, 5600 MB, the Netherlands
[b] Tata Steel, R&D, Microstructure & Surface Characterization (MSC), P.O. Box 10.000, 1970 CA, IJmuiden, the Netherlands
[c] School of Civil Engineering, Wuhan University, 430072, Wuhan, PR China

ARTICLE INFO

Keywords:
BOF slag
Hydration kinetics
Nanosilica
Potassium citrate

ABSTRACT

In this study, the early age hydration kinetics of BOF slag is investigated. Isothermal calorimetry and in-situ X-ray diffraction (XRD) are used to examine the effects of K_3-citrate concentration and nanosilica addition on slag reactivity. The results reveal that brownmillerite is the most reactive slag phase during the first 24 h of hydration. The kinetics of brownmillerite hydration is controlled by K_3-citrate dosage, and the reaction is strongly accelerated with highly concentrated solutions (0.6 M). A similar phenomenon is observed for amorphous C_2S at the early hydration stages. Among hydration products, crystalline siliceous hydrogarnet is identified. Precipitation of hydrogarnet (as observed with the XRD technique) coincidences well with the occurrence of a shoulder in the heat flow curves after the heat flow maximum due to brownmillerite dissolution. It is shown that nanosilica slightly delays the hydration of brownmillerite while enhancing the precipitation of C-S-H gel. In consequence, the early age mechanical properties of BOF slag mortars with nanosilica addition are improved.

1. Introduction

Annually, around 100–130 million tonnes of Basic Oxygen Furnace BOF slag (a by-product from steel manufacture) are generated worldwide (80–120 kg per tonne of steel) [1–3]. Therefore, the application of BOF slag in the concrete industry is of high interest [4]. Recent studies show that the BOF slag reveals a partial hydraulic activity and can be applied as a cementitious binder either when it is sufficiently ground or chemically activated [5–7]. BOF slag is composed of C_2S, wuestite, brownmillerite and magnetite, and minor phases including C_3S, free lime, portlandite and calcite [1,5,8–10]. The hydraulic properties of BOF slags mainly depend on the contents of C_2S and $C_2(A,F)$ and the reactivity of these phases. Even though C_2S constitutes about 50 wt% and brownmillerite about 20 wt% of slag, the reactivity of BOF slag tends to be low due to late hydraulic activity of C_2S and most likely due to its contamination with Fe^{3+}, P^{5+}, as well as the entrapment of reactive phases within the inert slag particles [5,7,11].

In cement systems, the reaction of brownmillerite takes place simultaneously with the reaction of C_3A at the very early hydration stages, while the reaction of C_2S contributes to the late strength development. Due to the late hydraulic activity of C_2S, early age mechanical properties of BOF slag-based materials might be insufficient for practical applications. In the work of Kaja and Yu [5], it was shown that the chemical activation of BOF slag with potassium citrate enables the increase of the overall hydration degree of BOF slag, which, together with the superplasticizing effect of potassium citrate, lead to the superior mechanical properties of BOF slag pastes, up to 75 MPa, after 28 days of hydration [5]. However, the impact of the early age phase development on mechanical properties has not yet been investigated.

A commonly applied strategy to increase the early-age strength development of hydrating cement and its composites with slag or pozzolanic materials is the addition of nanomaterials, particularly nanosilica [12,13]. Due to the amorphous nature and high specific surface area, nano-silica (nS) features a very high pozzolanic activity [14–16]. The accelerating function of nS is attributed to the provision of additional nucleation sites, and, as revealed more recently [17], to the rapid depletion of calcium ions from the pore solution. Nano-silica contributes not only to early strength development but also causes structural densification [18–21]. The structural refinement in the presence of nano-silica and the consequent durability improvement can be crucial for BOF slag-based systems, which are often contaminated with heavy metals (mainly vanadium and chromium) [1,5,22]. In the BOF slag system, nano-silica can potentially strengthen the structures of C–S–H gel and siliceous hydrogarnet- the main hydration products, which presumably host heavy metals [5,23].

Consequently, in this study, we aim to investigate the combined

* Corresponding author. Department of the Built Environment, Eindhoven University of Technology, Eindhoven, 5600 MB, the Netherlands.
E-mail address: q.yu@bwk.tue.nl (Q. Yu).

https://doi.org/10.1016/j.cemconcomp.2021.104262
Received 9 June 2020; Received in revised form 27 January 2021; Accepted 10 September 2021
Available online 22 September 2021

effects of nanosilica addition and tri-potassium citrate concentration on the early age hydration of BOF slag. The reaction kinetics and early phase assemblage, analysed with in-situ and ex-situ XRD measurements, isothermal calorimetry and thermogravimetric analyses, are related to the mechanical properties of BOF slag mortars. This strategy is used to optimize the strength development of slag-based materials and, at the same time, to increase their durability.

2. Experimental

2.1. Materials

A representative batch of BOF slag from the steel manufacture was collected and provided by Tata Steel (The Netherlands) and used in this study to perform the experiments. The slag (2–5.6 mm grains) was firstly ground with a vibratory disc mill (RS 300, Retsch). The particle size distribution of the milled slag, measured with the laser diffraction spectroscopy method (Mastersizer 2000, Malvern), is presented in Fig. 1.

The BOF slag was chemically and mineralogically analysed with the X-ray fluorescence (XRF) and the quantitative X-ray diffractometry (XRD), respectively. The results are presented in Table 1. The XRD-amorphous content in the BOF slag accounts mostly for the C_2S phase, as shown in our previous study [5].

Nanosilica, with 99.7% purity, was obtained through the dissolution of olivine (as described in detail in Refs. [24,25]). The specific surface area (measured with the BET method) and the specific density of the synthesized nano-silica were about 400 m^2/g and 2.0 g/cm^3, respectively. Tri-potassium citrate monohydrate ($K_3C_6H_5O_7{\cdot}H_2O$, GPR RECTAPUR®, purity > 99%) was employed with a dual role of activator and superplasticizer [5]. The CEN-standard sand was used for the preparation of mortars.

2.2. Mix design and sample preparation

The BOF slag pastes with and without the addition of nanosilica were prepared according to the mix design shown in Table 2. Nanosilica was applied by substituting 2 vol % of the slag. This relatively low dosage of nS was selected considering the high specific surface area (400 m^2/g) of nS and the content of the potentially reactive phases in BOF slag [26]. The concentrations of tri-potassium citrate were chosen based on our previous study [5].

For the preparation of pastes, nanosilica was firstly dispersed in 2/3 of water using the Hielscher UP400S ultrasonic device (15 min, with an amplitude of 75%). The temperature of the solutions was controlled with the ice water bath at the level of 21 ± 0.2 °C before application. The tri-potassium citrate monohydrate was dissolved in the remaining water. Both solutions were mixed with slag for 3 min using a high-speed mixer. Pastes were subsequently poured in the polyethylene vials and sealed cured (20 °C, RH>95%) until the designed testing ages.

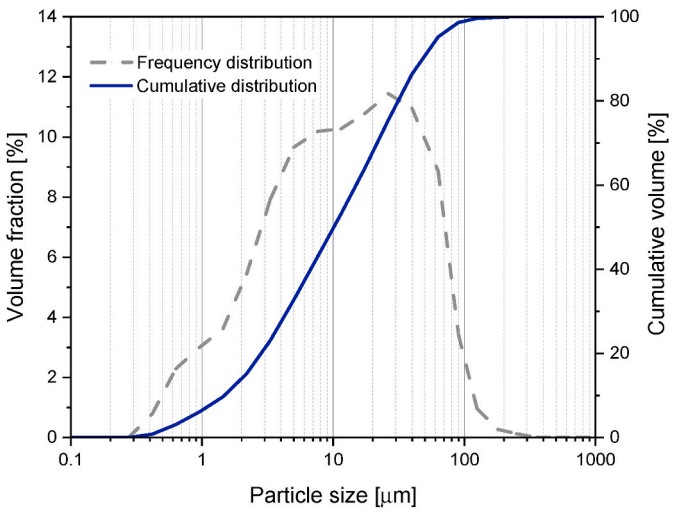

Fig. 1. The frequency and cumulative distribution of the particle size of the slag powder.

Table 1
Chemical and mineralogical characteristics of BOF slag.

Mineral compound	Content [wt%]	Oxide	Content [wt%]
Brownmillerite	20.8	**MgO**	6.0
Magnetite	9.7	**SiO_2**	12.0
C_2S	30.8	**Al_2O_3**	3.2
Wuestite	19.7	**CaO**	41.0
Lime	1.1	**P_2O_5**	1.4
Calcite	0.3	**TiO_2**	1.1
Portlandite	0.6	**V_2O_5**	1.1
C_3S	0.7	**Cr_2O_3**	0.3
Amorphous	16.3	**MnO**	4.7
		Fe_2O_3	29.0
		GOI 1000	0.14

Table 2
The compositions of the mixtures for the preparation of the paste.

Sample ID	BOF slag [g]	nS (olivine) [g]	Water [g]	Activator [M]	w/b (mass ratio)	w/b (volume ratio)
C0.2	100	–	18	0.2	0.180	0.66
C0.6	100	–	18	0.6	0.180	0.66
C0.2nS2	98	1.087	18	0.2	0.184	0.66
C0.6nS2	98	1.087	18	0.6	0.184	0.66

For the compressive strength evaluation, mortar prisms were prepared. To ensure sufficient workability of mortars (S4, according to EN 206-1), an additional amount of water was added, resulting in a water/binder mass ratio of 0.25. The sand content was adjusted to obtain a similar paste to sand volumetric ratio as for standard cement mortars (EN 196-1). In consequence, a sand to slag mass ratio of 2 was used. Mortars were prepared using a Hobart mixer following the procedure described in EN 196-1 but with extended mixing time (a total mixing time of 10 min was employed). Due to the high density of slag and the limited/late reactivity of the slag phases, bleeding problems were encountered during the samples' preparation. The impact of this phenomenon on the final results should be considered and requires further investigation as some signs of bleeding were also observed on the paste level.

2.3. Methodology

2.3.1. Isothermal calorimetry

The heat flow and cumulative heat release from the reacting BOF slag were monitored with an isothermal conduction calorimeter (TAM Air, Thermometric). The external mixing method was applied. Firstly, the tri-potassium citrate solution was prepared, and nanosilica was dispersed in water with an ultrasonic device. Then, both solutions were mixed with BOF slag for 2 min. Pastes were subsequently transferred to the glass ampoules and loaded into the calorimeter. The measurement temperature was set to 20 °C. For the evaluation of the total heat release, the integration of the heat flow curve was made from 45 min after the sample insertion, when the measurement conditions were stabilized.

2.3.2. XRD

Changes in the phase composition of the hydrating BOF slag pastes were monitored with the in-situ XRD method within the first 24 h of hydration. An X'Pert Pro PANalytical diffractometer in theta-theta geometry was used. For the preparation of pastes, the mixing procedure described in Section 2.2 was employed. Pastes were subsequently placed in the sample holders, flattened with a spatula, and covered with a

Kapton foil to minimize water evaporation and CO_2 ingress. The measurements were carried out with the settings listed in Table 3. Each diffraction pattern was recorded for about 15 min. At later hydration stages, the hydration of BOF slag pastes was arrested with the solvent exchange method (isopropanol, diethyl ether [27]). The XRD measurements were performed on the powder samples using a Bruker D4 ENDEAVOUR X-ray Diffractometer.

2.3.3. Thermogravimetric analysis

After hydration stoppage, the powders (around 50 mg) were thermally treated using a Jupiter STA 449 F1 Netzsch instrument, with the heating rate of 5 °C/min, in the temperature range between 40 and 1000 °C. A nitrogen atmosphere was employed.

2.3.4. Compressive strength

The compressive strength was evaluated on the mortar prisms (4 × 4 × 16 cm^3). Samples were demoulded after 24 h, and then sealed with plastic film, and cured in the controlled conditions of 20 °C, RH>95% until further testing. The strength measurements were performed following the EN 196-1 standard after 3, 7, and 28 days of curing, respectively.

2.3.5. XRD interpretation

Quantitative phase analysis was performed utilizing Rietveld refinement with the use of the TOPAS Academic software v5.0. The external standard method (corundum) was employed. This method enables the quantification of phases independently, which is especially important when hydration products reveal low crystallinity. The mass absorption coefficients of pastes were calculated based on the International Tables of Crystallography [28]. The crystal structures used for the Rietveld refinement are catalogued in Table 4, while described in more detail in our previous work [29]. The lattice parameters, crystallite size, and microstrain of the slag phases were determined on anhydrous slag and then used unrefined for the phase quantification in hydrating slag. The broad XRD hump caused by the Kapton film, free water, and amorphous content was modeled by introducing individual peaks. To account for the changes in the phase contents, the peak areas were refined, whereas the positions of the peaks were kept fixed. With the in-situ XRD method, only the pastes with 0.2 M K_3-citrate were investigated. Due to the high fluidity of the pastes with 0.6 M K_3-citrate and strongly alkaline pH of the pore solution [30], slight bleeding and deposition of carbonates (caused by partial destruction of the Kapton foil) were observed on the surface of the samples. It has to be noted that these factors might affect the quantitative interpretation of the results.

2.3.6. Heat flow calculation

To validate the findings regarding the early age reactions taking place in BOF slag pastes obtained with calorimetry and in-situ XRD, the measured heat flow curves from the isothermal calorimeter were compared with the heat flows calculated from the in-situ XRD experiments [31]. This method enables verification of the contribution of the dissolution/precipitation processes assigned to the particular phase in BOF slag to the overall heat release during the investigated period of the hydration. Based on the previous studies [32,33], the following equation was used to describe the reaction of brownmillerite, knowing that the composition of brownmillerite in BOF slag is slightly closer to C_2F than to C_4AF [8]:

$$Ca_2Fe_2O_5 + 5H_2O \rightarrow 2Ca^{2+} + 4OH^- + 2Fe(OH)_{3(am)} \quad (1)$$

$$\Delta H_{R(C_2F)} = -429.21\ [J/g]$$

The precipitation of iron (III) hydroxide was assumed to take place during the first hours of hydration, as indicated in Refs. [34,35], and later confirmed by Dilnesa et al. [36] for the C_4AF phase. During the hydration of C_2F, similar behaviour is expected. The formation of iron (III) hydroxides was previously observed upon hydration of C_2F phase [37].

The enthalpy of the C_2F reaction was determined using the thermodynamic data listed in Table 5. In the next step, the heat flow was calculated according to equation (2) [32]. For the calculations, the phase contents derived from the XRD measurements were smoothed with a Fourier filter [31].

$$HF_i(t) = \frac{dc_i(t)}{dt} \cdot \Delta H_{R\ (i)} \quad (2)$$

Where:

$HF_i(t)$ is the heat flow of phase i [mW/g] at the time t [h]
$c_i(t)$ is the content of phase i [wt. %] at the time t [h]
$\Delta H_{R\ (i)}$ is the enthalpy of reaction of phase i [J/g]

Table 3
Instrumental parameters for in-situ and ex-situ XRD measurements.

Parameter	Value	
	In-situ XRD	XRD on powder samples
Device	X'Pert Pro PANalytical	D4, Bruker AXS
X-ray tube	Co	Co
Voltage/Current	35 kV/45 mA	40 kV/40 mA
Detector	PIXcel^{3D}	LynxEye
Scan range	10–70 °2θ	10–80 °2θ
Step size	0.026 °2θ	0.014 °2θ
Time per step	0.41 s	1 s

Table 4
ICSD codes of the crystal structures used in the Rietveld refinement.

Phase	ICSD
Brownmillerite	9197[a]
Magnetite	20596
Wuestite	67200[a]
β-C_2S	245074
α′-C_2S	81097
C_3S	64759
Lime	28905
Portlandite	202220
Hydroandradite	29247[a]
Katoite	9272[a]
Pyroaurite	6295

[a] The compositions were adjusted based on [29].

3. Results and discussion

3.1. Hydration kinetics

The hydration kinetics of BOF slag is strongly affected by the dosage of tri-potassium citrate, as already shown in more detail in our previous studies [5,29]. From Fig. 2, it can be seen that the change of K_3-citrate concentration from 0.2 M to 0.6 M results in the elimination of the induction period, which lasts about 4 h for paste with 0.2 M K_3-citrate. The shape of the "main peak" of the heat flow curve, associated with the reaction of BOF slag phases, is broader for a higher activator dosage, and

Table 5
Enthalpies of formation used for the calculation of the heat flow.

Phase/species	ΔH_f[kJ/mol]	Reference
$Ca_2Fe_2O_5$	−2124.22	*Recalculated from* [38]
H_2O	−285.88	[39]
Ca^{2+}	−543.07	[39]
OH^-	−230.01	[39]
$Fe(OH)_{3(am)}$	−832	[39]

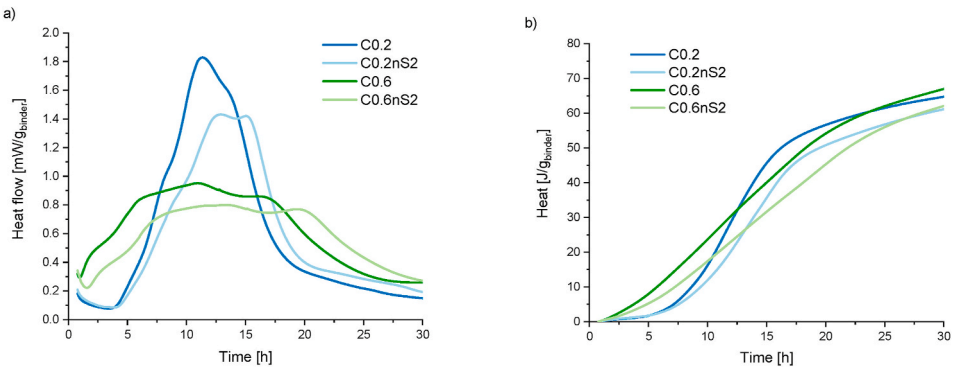

Fig. 2. The isothermal calorimetry results of the investigated mixtures a) heat flow and b) cumulative heat.

the total amount of the heat released during the first 24 h is slightly higher than for paste with 0.2 M citrate. With the addition of 2% of nanosilica, for both K_3-citrate concentrations, the hydration of BOF slag is delayed.

The retarding effect of nanosilica observed in our systems contradicts the accelerating function of nS in Portland cement systems [40]. During the hydration of Portland cement, nanosilica accelerates the reaction by offering additional nucleation sites and/or boosting the depletion of calcium ions from the pore solution. However, these effects seem to be outbalanced by other phenomena when BOF slag is activated by K_3-citrate. One of the postulates is that potassium citrate interacts with nanosilica, and therefore, its availability to enhance the dissolution of BOF slag phases is lowered. Since at the early hydration stages, the pH of the pore solution of BOF slag paste is strongly affected by the K_3-citrate dosage (ranging from ~12.8 for 0.1 M to 13.4 for 0.6 M during the first 30 min of hydration [30]), the retardation effect can also be caused by a slight decrease of pH in the presence of nanosilica.

3.2. Phase assemblage

The changes in the phase composition of BOF slag pastes upon hydration are presented in Table 5. The quantitative XRD analyses reveal that at the early hydration stages, brownmillerite is the most reactive phase in BOF slag. The reaction of brownmillerite occurs mainly within the first day of hydration regardless of the concentration of potassium citrate. A greater extent of brownmillerite reaction is observed for the pastes with 0.6 M K_3-citrate than pastes with 0.2 M K_3-citrate. The addition of nanosilica results in a slightly delayed dissolution of this phase.

Next to brownmillerite, partial dissolution of wuestite is observed. The reactivity of wuestite, examined with the XRD method, might be overestimated due to the sample preparation procedure, as discussed in detail in Ref. [29]. In all pastes, the magnetite is relatively inert during the investigated hydration period. The crystalline C_2S reacts to a limited extent within 28 days of hydration, showing a slightly higher reaction degree when a lower dosage of K_3-citrate is applied. The main crystalline product of BOF slag hydration is siliceous hydrogarnet (Hg) [5]. Additionally, the formation of pyroaurite ($Mg_6Fe^{3+}_2(OH)_{16}[CO_3]\cdot 4H_2O$) was detected with a broad reflection at $2\theta = 13.5^{\circ}$, in agreement with our previous study [5]. Due to the very low contents and poorly crystalline structure of this phase, it is not included in Table 6.

3.3. Hydration of brownmillerite

Since brownmillerite is the most reactive crystalline phase in the examined systems and its reaction occurs mostly during the first 24 h of hydration, the reaction kinetics of this phase becomes crucial for the setting time of pastes and their early age mechanical properties. In-situ XRD experiments were carried out to reveal the impact of nanosilica addition on the reaction kinetics of brownmillerite.

Fig. 3 shows the phase evolution in hydrating BOF slag paste with 0.2 M potassium citrate with and without the addition of nanosilica. It can be seen that brownmillerite shows the highest reactivity among other phases and that the precipitation of hydrogarnets follows its hydration. A slight delay is observed in the system with nanosilica. Similar behaviour is expected for BOF slag paste with 0.6 M K_3-citrate.

Table 6
The phase composition of the BOF slag pastes after selected hydration periods.

	Time (day)	$C_2(A,F)$	C_2S	C_3S	Wuestite	Magnetite	Lime	CH	Cc	Hg
C0.2	0	20.8	30.8	0.7	19.7	9.7	1.1	0.6	0.3	0.0
	1	10.2	29.2	0.7	17.5	9.0	0.5	1.1	0.1	10.5
	3	9.8	28.7	0.7	16.7	8.5	0.6	1.3	0.1	10.9
	7	10.2	27.7	0.7	16.8	8.7	0.6	1.7	0.2	11.0
	28	9.7	22.5	0.5	18.5	8.6	0.5	2.1	0.3	12.7
C0.2nS2	0	20.6	30.5	0.7	19.5	9.6	1.1	0.6	0.3	0.0
	1	10.9	29.8	0.7	16.8	8.9	0.6	0.8	0.2	8.8
	3	10.7	30.8	0.7	15.8	8.7	0.5	0.9	0.2	9.0
	7	10.1	28.5	0.8	16.1	8.7	0.5	0.9	0.2	9.8
	28	9.6	24.7	0.7	16.9	8.8	0.5	1.1	0.3	11.2
C0.6	0	20.8	30.8	0.7	19.7	9.7	1.1	0.6	0.3	0.0
	1	6.5	27.6	1.1	16.9	8.4	0.4	1.0	0.4	10.9
	3	5.4	28.1	0.8	13.9	8.5	0.5	1.0	0.2	13.4
	7	5.6	27.9	0.8	13.2	8.4	0.4	1.2	0.1	14.1
	28	4.8	26.3	0.7	11.9	8.3	0.3	1.8	0.2	15.5
C0.6nS2	0	20.6	30.5	0.7	19.5	9.6	1.1	0.6	0.3	0.0
	1	7.0	29.6	0.7	16.4	8.5	0.4	0.6	0.2	7.8
	3	5.7	28.5	0.8	15.1	8.5	0.5	0.6	0.2	11.4
	7	5.4	28.1	0.7	13.8	8.6	0.4	0.7	0.2	12.2
	28	5.0	26.2	0.8	13.1	8.4	0.5	0.7	0.3	13.3

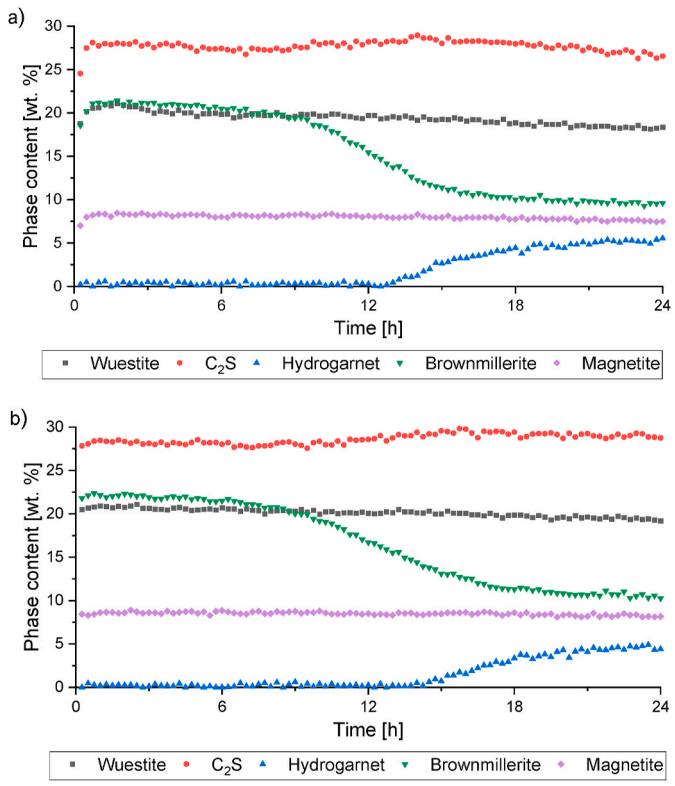

Fig. 3. Phase development for BOF slag pastes a) C0.2, and b) C0.2nS2, derived from the in-situ XRD measurements.

Calorimetry data indicate that the dissolution of brownmillerite in that system takes place immediately after contact with water.

A comparison between the calorimetry and in-situ XRD results (Fig. 4) shows that the shoulder on the heat flow curve on the right side of the main reaction peak (at around 13 h for paste without nS and 15 h for paste with nS) coincidences well with the precipitation of hydrogarnets. The exact composition of hydrogarnets ($Ca_3(Al_xFe_{1-x})_2(SiO_4)_y(OH)_{4(3-y)}$) is difficult to establish as it can form solid solutions [23]. The gradual uptake of SiO_4^- in the structure of hydrogarnets is commonly observed [41]. Therefore, simplifications are required for the quantification of this phase, as described in Ref. [5]. The presented data show clear evidence for the formation of hydrogarnets in the investigated BOF slag systems. However, further studies are required to better understand the exact nature of this hydration product. Interestingly, the precipitation of crystalline hydrogarnets was not observed in the previous studies on the early hydration of synthesized brownmillerite [32,33]. Even though it was shown that the majority of brownmillerite underwent dissolution during the initial 24 h of hydration (either with or without the presence of gypsum), the formation of silicon-free hydrogarnets was not observed. On the other hand, for Portland cement paste, the precipitation of hydrogarnets was detected after 16 h of hydration [36]. This behavior indicates that the presence of silicate ions and/or pH of the pore solution are critical factors for the precipitation of crystalline hydrogarnets (at the early hydration stages). For matured Portland cement systems, siliceous hydrogarnets are considered the most stable iron-containing hydrates, being the reaction products of brownmillerite and C_2S/C_3S [42,43].

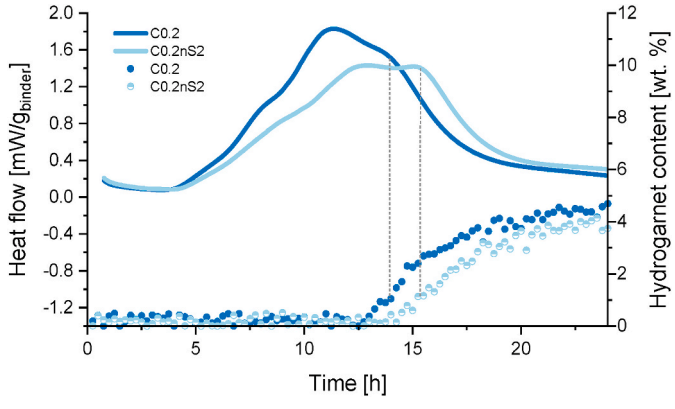

Fig. 4. Heat flow curves derived from the calorimetry measurements and hydrogarnet content during hydration of slag in C0.2 and C0.2nS2.

3.4. Hydration of silicate

Since part of C_2S in BOF slag is XRD-amorphous [5] and its potential reaction is not detectable with the XRD method, the heat flow curves from calorimetric measurements were compared with the curves calculated from in-situ XRD data. The brownmillerite was considered the only hydrating crystalline phase during the first 24 h of hydration (see Fig. 3). The slight dissolution of other crystalline phases (as shown in Table 6) was not taken into account, being assigned mostly to the initial dissolution (after contact with water), which is not analysed in this study. Fig. 5 reveals good agreement between the measured and calculated heat flow curves for pastes with 0.2 M of potassium citrate. The satisfactory correspondence regarding the positions (time) and shapes of the curves confirms that the evolved heat is mainly due to the reaction of brownmillerite. The difference between the measured and calculated heat can be explained by the presence of aluminum in brownmillerite (which is not considered in the proposed reaction) but also likely originates from the dissolution of amorphous C_2S and precipitation of hydrogarnet. It is generally accepted that α′-C_2S polymorph, which coexists in BOF slag with β-C_2S (commonly observed in Portland cement), reveals a higher reactivity than β-polymorph. Knowing that the potassium citrate is boosting the pH of the pore solution [30], the early age dissolution of this phase is expected to occur, especially in samples with 0.6 M K_3-citrate [5,44].

To further support this hypothesis, thermogravimetric measurements were conducted. The mass loss due to the dehydration of C–S–H gel after selected hydration times was used to indicate the differences in the extent of C_2S reaction in the investigated pastes. Similarly, the precipitation of hydrogarnets, resulting from the reaction of

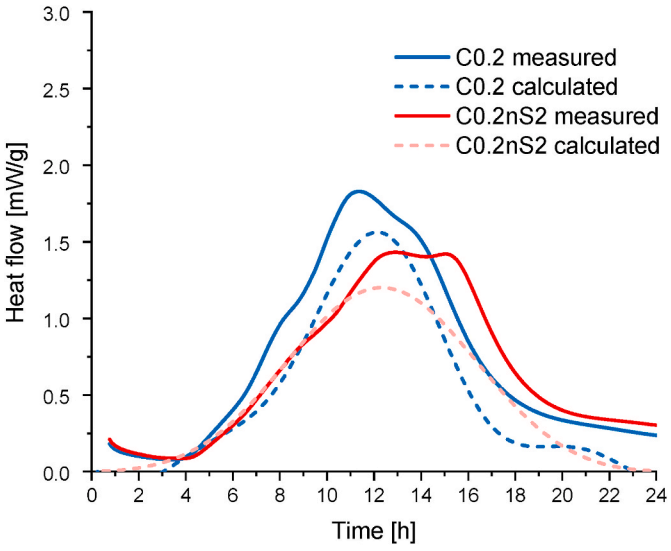

Fig. 5. The comparison of the heat flow of hydrating BOF slag pastes measured with isothermal calorimetry and the heat flow calculated from the reaction of C_2F based on the in-situ XRD data.

brownmillerite and C_2S, was followed. An exemplary DTG curve is shown in Fig. 6 a).

For the hydrated BOF slag, the mass loss occurs due to the decomposition of C–S–H gel, hydrogarnets, pyroaurite, portlandite, and carbonates/citrate compounds. It is widely reported that the dehydration of C–S–H gel in cement paste takes place within a broad temperature range (up to 400/500 °C), with the main water release at around 100 °C [45,46]. For the gel products of alkali activation, with aluminum and alkali metals in the structure, the water loss is observed within a similar temperature range [47]. At the same time, depending on the chemical composition, the decomposition of hydrogarnets occurs between 200 and 400 °C [23]. Pyroaurite decomposes between 180 and 410 °C [48] and portlandite between 400 and 500 °C [27]. Overlapping of the temperature ranges in which the water is released from different hydration products precludes the quantitative analysis of the results. Nevertheless, based on the literature and the shape of DTG curves observed for hydrated BOF slag, the temperature intervals assigned to the water loss from different hydration products were selected to demonstrate the differences in the hydration kinetics of slag phases. As presented in Fig. 6 a), it was assumed that mass loss between 40 and 180 °C originates mostly from the dehydration of C–S–H gel, whereas between 180 and 410 °C from the dehydration of hydrogarnet and, to a smaller extent, pyroaurite. Additionally, the total mass loss due to the water release was analysed in the range between 40 and 500 °C, as recommended in Ref. [27]. It has to be noted, however, that the presented temperature ranges cannot be exclusively assigned to the decomposition of a particular hydration product (e.g., decomposition of C–S–H gel takes place up to 500 °C) and therefore have only indicative character.

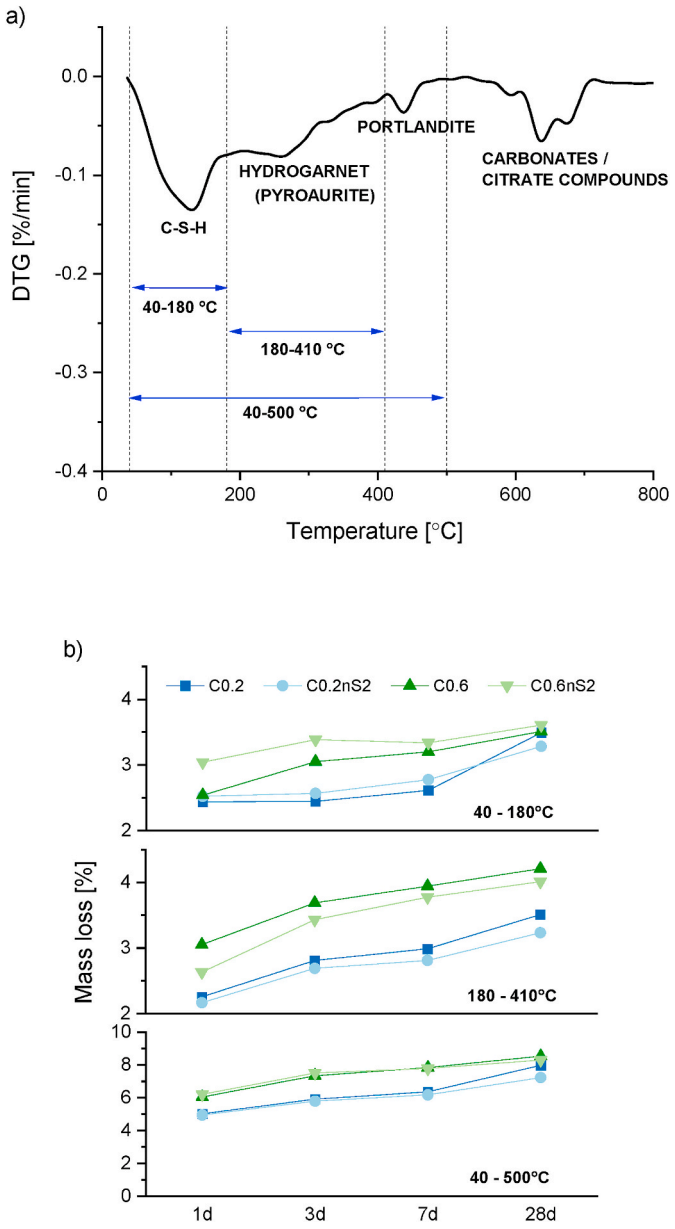

Fig. 6. The thermogravimetric results showing a) the exemplary DTG curve of hydrated BOF slag b) the mass loss from BOF slag pastes due to the water release within the selected temperature intervals.

From Fig. 6 b), it can be seen that the mass loss between 40 and 180 °C is generally higher for BOF slag pastes with 0.6 M of K_3-citrate during the first 7 days of hydration, indicating a greater extent of C_2S reaction in these samples. This behaviour can be directly related to the higher pH of the pore solution during the early hydration of BOF slag in pastes with 0.6 M of K_3-citrate in comparison to the pastes with 0.2 M of K_3-citrate [30]. Furthermore, the addition of nanosilica results in the enhanced precipitation of C–S–H gel. This observation strongly suggests that nanosilica is consumed in the pozzolanic reaction, resulting in lower portlandite contents (as shown in Table 6), rather than being incorporated in the structure of hydrogarnet.

However, the accelerating effects of pH and nS addition are less pronounced after 28 days of hydration, which is especially evident for the pastes with 0.2 M of K_3-citrate, in which a higher mass loss is observed for the sample without nanosilica. Similarly, the differences in the mass loss between the pastes with the two analysed dosages of potassium citrate are minimized or eliminated at this age. The above-mentioned observations bring us to the conclusion that the enhanced early age hydration of C_2S adversely affectss the late reaction of this phase.

The mass losses in the temperature range between 180 and 410 °C, mostly due to dehydration of hydrogarnets, correlate well with the findings from the XRD analyses. The mass loss is substantially higher for the pastes with 0.6 M of K_3-citrate than for pastes with 0.2 M of K_3-citrate. For both activator dosages, the delayed reaction of brownmillerite and consequent precipitation of hydrogarnets are also reflected in the presence of nanosilica.

At the same time, the total mass loss due to the water release from the hydration products shows the combination of the two opposite effects of nanosilica, which enhances the precipitation of C-S-H gel while having a negative impact on the hydration of brownmillerite at the early hydration ages. In consequence, no substantial differences in the bound water content between the reference samples and the samples containing nanosilica are observed. Nonetheless, it is worth mentioning that after 28 days of hydration, the samples without nanosilica addition tend to contain more chemically bound water.

3.5. Mechanical performance

In our previous study, we have shown that the BOF slag paste can reach a strength of up to 75 MPa after 28 days of hydration (when 0.2 M potassium citrate is applied) [29]. However, it has been often reported that for alkali/chemically activated binders, the transition from paste to mortar causes a significant decline in performance due to higher water demand [49]. In this study, the mechanical performance was investigated on the mortar samples, and therefore, additional water had to be added to the mixtures to provide sufficient flowability. In consequence, the potassium citrate solutions were diluted, and the kinetics of BOF slag hydration was affected. Nevertheless, the observed changes in the mechanical performance provide significant insight into the effects of early slag hydration kinetics on the later phase development, especially the hydration of C_2S (the most abundant phase in BOF slag).

Fig. 7 shows the compressive strength results for the BOF slag mortars. The mortars with 0.6 M potassium citrate reveal accelerated

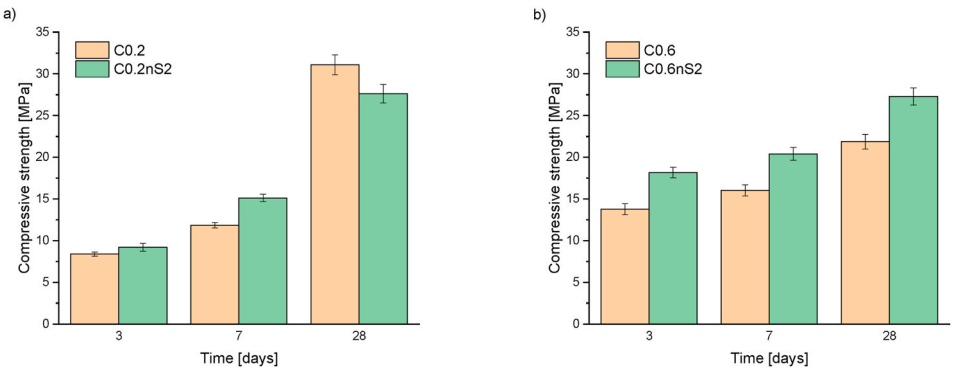

Fig. 7. The compressive strength of BOF slag mortars after selected curing periods.

strength development in comparison to the mortars with 0.2 M K_3-citrate. After 3 and 7 days of curing, the difference in the strength of 64% and 35% is observed, respectively. After 28 days, however, higher compressive strength is reported for mortars with a lower concentration of potassium citrate. The addition of nanosilica improves the compressive strength of mortars with 0.6 M K_3-citrate after all the investigated curing periods. For mortars with 0.2 M K_3-citrate, strength increase is observed after 3 and 7 days, while after 28 days, mortars with nanosilica show a decline in strength compared to the reference samples.

The XRD and thermogravimetric analyses disclose that nanosilica delays the hydration of brownmillerite and enhances the precipitation of C-S-H gel. Furthermore, it is revealed that in the pastes with 0.6 M of K_3-citrate, the early hydration of amorphous C_2S is promoted. The improved early-age performance of BOF slag mortars with the higher activator dosage and with nS addition at the early hydration stages indicates that the C–S–H gel is a principal strength-giving phase, whereas hydrogarnets have a lesser impact on the mechanical properties of BOF slag mortars. Furthermore, the increased early age reactivity of C_2S seems to have a negative influence on its overall hydration degree, and therefore, after 28 days of hydration, the highest mechanical performance is observed for the mortar without nanosilica and with a low concentration of K_3-citrate.

4. Conclusions

This work focuses on the early age hydration of BOF slag. Special attention is paid to the impact of nanosilica and K_3-citrate concentration on the hydration kinetics of the slag phases. The compositional changes in the slag pastes are related to the mechanical properties of mortars. The following conclusions are reached.

- The early hydration of BOF slag activated with K_3-citrate is dominated by the reaction of brownmillerite and, to a lesser extent, of amorphous C_2S, leading primarily to the formation of hydrogarnets and C–S–H gel.
- The kinetics of the brownmillerite reaction can be controlled by adjusting the dosage of potassium citrate (where hydration is accelerated about 4 h for samples with 0.6 M K_3-citrate compared to the samples with 0.2 M K_3-citrate).
- Highly concentrated solutions of K_3-citrate increase the early age reactivity of C_2S.
- Silica nanoparticles (at the dosage of 2 vol %) delay the reaction of brownmillerite while enhancing the formation of C-S-H gel.
- Mortars with nS addition and highly concentrated potassium citrate solutions (0.6 M) exhibit improved early age mechanical properties. Increased compressive strength is associated with accelerated hydration of C_2S / precipitation of C-S-H gel. However, up to 28 days, the strength development becomes insubstantial for these samples, likely due to the suppressed reaction of C_2S.

Declaration of competing interest

The authors declare that they have no known competing financial interests or personal relationships that could have appeared to influence the work reported in this paper.

Acknowledgment

The authors would like to acknowledge the financial support by NWO (The Netherlands Organisation for Scientific Research) for funding this research (project no. 12824).

References

[1] A. van Zomeren, S.R. van der Laan, H.B.A. Kobesen, W.J.J. Huijgen, R.N. J. Comans, Changes in mineralogical and leaching properties of converter steel slag resulting from accelerated carbonation at low CO2pressure, Waste Manag. 31 (11) (2011) 2236–2244, https://doi.org/10.1016/j.wasman.2011.05.022.
[2] S.Z. Carvalho, F. Vernilli, B. Almeida, M. Demarco, S.N. Silva, The recycling effect of BOF slag in the portland cement properties, Resour. Conserv. Recycl. 127 (September) (2017) 216–220, https://doi.org/10.1016/j.resconrec.2017.08.021.
[3] Steel statistical yearbook 2020 concise version. https://www.worldsteel.org/en/dam/jcr:5001dac8-0083-46f3-aadd-35aa357acbcc/SSY%25202020_concise%2520version.pdf. (Accessed 7 January 2021) accessed.
[4] S. Zhuang and Q. Wang, "Inhibition mechanisms of steel slag on the early-age hydration of cement," Cement Concr. Res., vol. 140, p. 106283, Feb. 2021, doi: 10.1016/j.cemconres.2020.106283.
[5] A. M. Kaja and Q. L. Yu, WO2020188070 (A1) - “Method for the manufacture of high-end performance steel slag-based building products”, 24-09-2020.
[6] J. Zhao, D. Wang, P. Yan, D. Zhang, H. Wang, Self-cementitious property of steel slag powder blended with gypsum, Construct. Build. Mater. 113 (2016) 835–842, https://doi.org/10.1016/j.conbuildmat.2016.03.102.
[7] S. Kourounis, S. Tsivilis, P.E. Tsakiridis, G.D. Papadimitriou, Z. Tsibouki, Properties and hydration of blended cements with steelmaking slag, Cement Concr. Res. 37 (6) (2007) 815–822, https://doi.org/10.1016/j.cemconres.2007.03.008.
[8] C. van Hoek, J. Small, S. van der Laan, Large-area phase mapping using PhAse recognition and characterization (PARC) software, Micros. Today 24 (5) (2016) 12–21, https://doi.org/10.1017/S1551929516000572.
[9] F. Han, Z. Zhang, Properties of 5-year-old concrete containing steel slag powder, Powder Technol. 334 (2018) 27–35, https://doi.org/10.1016/j.powtec.2018.04.054.
[10] J. Li, Q. Yu, J. Wei, T. Zhang, Structural characteristics and hydration kinetics of modified steel slag, Cement Concr. Res. 41 (3) (2011) 324–329, https://doi.org/10.1016/j.cemconres.2010.11.018.
[11] Y. Jiang, T.C. Ling, C. Shi, S.Y. Pan, Characteristics of steel slags and their use in cement and concrete—a review, Resour. Conserv. Recycl. 136 (2018) 187–197, https://doi.org/10.1016/j.resconrec.2018.04.023. December 2017.
[12] M.H. Zhang, J. Islam, S. Peethamparan, Use of nano-silica to increase early strength and reduce setting time of concretes with high volumes of slag, Cement Concr. Compos. 34 (5) (2012) 650–662, https://doi.org/10.1016/j.cemconcomp.2012.02.005.
[13] G. Land, D. Stephan, Controlling cement hydration with nanoparticles, Cement Concr. Compos. 57 (2015) 64–67, https://doi.org/10.1016/j.cemconcomp.2014.12.003.
[14] K. Sobolev, I. Flores, R. Hermosillo, L.M. Torres-Martínez, Nanomaterials and nanotechnology for high-performance cement composites, in: In American Concrete Institute, ACI Special Publication, 2008, pp. 93–120, no. 254 SP.
[15] M. Amin, K. Abu El-Hassan, Effect of using different types of nano materials on mechanical properties of high strength concrete, Construct. Build. Mater. 80 (2015) 116–124, https://doi.org/10.1016/j.conbuildmat.2014.12.075.

[16] J. I. Tobón, J. Payá, and O. J. Restrepo, "Study of durability of Portland cement mortars blended with silica nanoparticles," Construct. Build. Mater., vol. 80, pp. 92–97, Apr. 2015, doi: 10.1016/j.conbuildmat.2014.12.074.
[17] D. Kong, D.J. Corr, P. Hou, Y. Yang, S.P. Shah, Influence of colloidal silica sol on fresh properties of cement paste as compared to nano-silica powder with agglomerates in micron-scale, Cement Concr. Compos. 63 (Oct. 2015) 30–41, https://doi.org/10.1016/j.cemconcomp.2015.08.002.
[18] A. Hanif, P. Parthasarathy, H. Ma, T. Fan, and Z. Li, "Properties improvement of fly ash cenosphere modified cement pastes using nano silica," Cement Concr. Compos., vol. 81, pp. 35–48, Aug. 2017, doi: 10.1016/j.cemconcomp.2017.04.008.
[19] H.S. Lee, B. Balasubramanian, G.V.T. Gopalakrishna, S.J. Kwon, S.P. Karthick, V. Saraswathy, Durability performance of CNT and nanosilica admixed cement mortar, Construct. Build. Mater. 159 (2018) 463–472, https://doi.org/10.1016/j.conbuildmat.2017.11.003. Jan.
[20] C. Nunes, Z. Slížková, M. Stefanidou, J. Němeček, Microstructure of lime and lime-pozzolana pastes with nanosilica, Cement Concr. Res. 83 (2016) 152–163, https://doi.org/10.1016/j.cemconres.2016.02.004.
[21] G. Quercia, G. Hüsken, H.J.H. Brouwers, Water demand of amorphous nano silica and its impact on the workability of cement paste, Cement Concr. Res. 42 (2) (2012) 344–357, https://doi.org/10.1016/j.cemconres.2011.10.008.
[22] L. De Windt, P. Chaurand, J. Rose, Kinetics of steel slag leaching: batch tests and modeling, Waste Manag. 31 (2) (2011) 225–235, https://doi.org/10.1016/j.wasman.2010.05.018.
[23] B.Z. Dilnesa, B. Lothenbach, G. Renaudin, A. Wichser, D. Kulik, Synthesis and characterization of hydrogarnet Ca3(AlxFe1 - X)2(SiO4)y(OH)4(3 - y), Cement Concr. Res. 59 (2014) 96–111, https://doi.org/10.1016/j.cemconres.2014.02.001.
[24] A. Lazaro, H.J.H. Brouwers, G. Quercia, J.W. Geus, The properties of amorphous nano-silica synthesized by the dissolution of olivine, Chem. Eng. J. 211–212 (2012) 112–121, https://doi.org/10.1016/j.cej.2012.09.042. Nov.
[25] A. Lázaro García, Nano-silica Production at Low Temperatures from the Dissolution of Olivine, Eindhoven University of Technology, 2014. PhD Thesis.
[26] Q. Bianchi, Application of Nano-Silica in Concrete, PhD Thesis, Eindhoven University of Technology, 2014.
[27] K. Scrivener, R. Snellings, B. Lothenbach, A Practical Guide to Microstructural Analysis of Cementitious Materials, 2018.
[28] third ed., in: E. Prince (Ed.), International Tables for Crystallography, C, International Union of Crystallography, 2006.
[29] A.M. Kaja, K. Schollbach, S. Melzer, S.R. van der Laan, H.J.H. Brouwers, Q. Yu, Hydration of potassium citrate-activated BOF slag, Cement Concr. Res. 140 (2021) 106291, https://doi.org/10.1016/j.cemconres.2020.106291. Feb.
[30] A. Kaja, A. Delsing, H. J. H. Brouwers, and Q. L. Yu, "Effects of Carbonation on the Retention of Heavy Metals in Chemically Activated BOF Slag Pastes," (no. Manuscript in preparation).
[31] C. Hesse, F. Goetz-Neunhoeffer, J. Neubauer, A new approach in quantitative in-situ XRD of cement pastes: correlation of heat flow curves with early hydration reactions, Cement Concr. Res. 41 (1) (2011) 123–128, https://doi.org/10.1016/j.cemconres.2010.09.014.
[32] D. Ectors, J. Neubauer, F. Goetz-Neunhoeffer, The hydration of synthetic brownmillerite in presence of low Ca-sulfate content and calcite monitored by quantitative in-situ-XRD and heat flow calorimetry, Cement Concr. Res. 54 (2013) 61–68, https://doi.org/10.1016/j.cemconres.2013.08.011.
[33] T. Hertel, J. Neubauer, F. Goetz-Neunhoeffer, Study of hydration potential and kinetics of the ferrite phase in iron-rich CAC, Cement Concr. Res. 83 (2016) 79–85, https://doi.org/10.1016/j.cemconres.2016.01.004.
[34] D.E. Rogers, L.P. Aldridge, Hydrates of calcium ferrites and calcium aluminoferrites, Cement Concr. Res. 7 (4) (1977) 399–409, https://doi.org/10.1016/0008-8846(77)90068-0.
[35] J.M. Fortune, J.M.D. Coey, Hydration products of calcium aluminoferrite, Cement Concr. Res. 13 (5) (1983) 696–702, https://doi.org/10.1016/0008-8846(83)90060-1.
[36] B.Z. Dilnesa, E. Wieland, B. Lothenbach, R. Dähn, K.L. Scrivener, Fe-containing phases in hydrated cements, Cement Concr. Res. 58 (2014) 45–55, https://doi.org/10.1016/j.cemconres.2013.12.012.
[37] H.F.W. Taylor, in: Cement Chemistry, second ed., Thomas Telford, London, 1997.
[38] E. Aleshin (Ed.), Proceedings of the Mineral Waste Utilization Symposium, IITRI, Chicago, Illinois, 1976.
[39] B. Lothenbach, et al., Cemdata18: a chemical thermodynamic database for hydrated Portland cements and alkali-activated materials, Cement Concr. Res. 115 (2019) 472–506, https://doi.org/10.1016/j.cemconres.2018.04.018. October 2017.
[40] H. Madani, A. Bagheri, T. Parhizkar, The pozzolanic reactivity of monodispersed nanosilica hydrosols and their influence on the hydration characteristics of Portland cement, Cement Concr. Res. 42 (12) (Dec. 2012) 1563–1570, https://doi.org/10.1016/j.cemconres.2012.09.004.
[41] V. Morin, P. Termkhajornkit, B. Huet, G. Pham, Impact of quantity of anhydrite, water to binder ratio, fineness on kinetics and phase assemblage of belite-ye'elimite-ferrite cement, 2017, Cement Concr. Res. 99 (2015) 8–17, https://doi.org/10.1016/j.cemconres.2017.04.014. no. December.
[42] H.J.H. Brouwers, A Hydration Model of Portland Cement Using the Work of Powers and Brownyard, Eindhoven University of Technology, Skokie, Illinois, U.S., 2011.
[43] H.F.W. Taylor, D.E. Newbury, An electron microprobe study of a mature cement paste, Cement Concr. Res. 14 (4) (1984) 565–573, https://doi.org/10.1016/0008-8846(84)90134-0.
[44] E. Belhadj, C. Diliberto, A. Lecomte, Characterization and activation of basic oxygen Furnace slag, Cement Concr. Compos. 34 (1) (2012) 34–40, https://doi.org/10.1016/j.cemconcomp.2011.08.012.
[45] A.V. Soin, L.J.J. Catalan, S.D. Kinrade, A combined QXRD/TG method to quantify the phase composition of hydrated Portland cements, Cement Concr. Res. 48 (2013) 17–24, https://doi.org/10.1016/j.cemconres.2013.02.007.
[46] Y. Wei, W. Yao, X. Xing, M. Wu, Quantitative evaluation of hydrated cement modified by silica fume using QXRD, 27Al MAS NMR, TG-DSC and selective dissolution techniques, Construct. Build. Mater. 36 (2012) 925–932, https://doi.org/10.1016/j.conbuildmat.2012.06.075.
[47] A.M. Kaja, A. Lazaro, Q.L. Yu, Effects of Portland cement on activation mechanism of class F fly ash geopolymer cured under ambient conditions, Construct. Build. Mater. 189 (2018) 1113–1123, https://doi.org/10.1016/j.conbuildmat.2018.09.065.
[48] K. Rozov, et al., Synthesis and characterization of the LDH hydrotalcite-pyroaurite solid-solution series, Cement Concr. Res. 40 (8) (2010) 1248–1254, https://doi.org/10.1016/j.cemconres.2009.08.031.
[49] X. Gao, Q.L. Yu, H.J.H. Brouwers, Properties of alkali activated slag-fly ash blends with limestone addition, Cement Concr. Compos. 59 (May 2015) 119–128, https://doi.org/10.1016/j.cemconcomp.2015.01.007.